Route to polarization switching induced by optical injection in vertical-cavity surface-emitting lasers

M. Sciamanna[1,*] and K. Panajotov[2,†]
[1]*Supélec, Laboratoire Matériaux Optiques, Photonique et Systèmes (LMOPS), CNRS UMR-7132, Unité de Recherche Commune Supélec et Université de Metz, 2 Rue Edouard Belin, F-57070 Metz, France*
[2]*Department of Applied Physics and Photonics (TW-TONA), Vrije Universiteit Brussel (VUB), Pleinlaan 2, B-1050 Brussels, Belgium*
(Received 22 September 2005; published 14 February 2006)

We perform a theoretical investigation of the polarization dynamics in a vertical-cavity surface-emitting laser (VCSEL) subject to orthogonal optical injection, i.e., the injected field has a linear polarization (LP) orthogonal to that of the free-running VCSEL. In agreement with previous experiments [Z. G. Pan *et al.*, Appl. Phys. Lett. **63**, 2999 (1993)], an increase of the injection strength may lead to a polarization switching accompanied by an injection locking. We find that this route to polarization switching is typically accompanied by a cascade of bifurcations to wave-mixing dynamics and time-periodic and possibly chaotic regimes. A detailed mapping of the polarization dynamics in the plane of the injection parameters (detuning, injection strength) unveils a large richness of dynamical scenarios. Of particular interest is the existence of another injection-locked solution for which the two LP modes both lock to the master laser frequency, i.e., an elliptically polarized injection-locked (EPIL) steady state. Modern continuation techniques allow us to unveil an unfolding mechanism of the EPIL solution as the detuning varies and also to link the existence of the EPIL solution to a resonance condition between the master laser frequency and the free-running frequency of the normally depressed LP mode in the slave laser. We furthermore report an additional case of bistability, in which the EPIL solution may coexist with the second injection-locked solution (the one being locked to the master polarization). This case of bistability is a result of the interaction between optical injection and the two-polarization-mode characteristics of VCSEL devices.

DOI: 10.1103/PhysRevA.73.023811 PACS number(s): 42.65.Sf, 05.45.−a, 42.55.Px

I. INTRODUCTION

The dynamics of semiconductor lasers is well known to be strongly affected by external perturbations [1] such as large current modulation [2] or the injection of external light, either from the laser itself (optical feedback) [3] or from an external laser (optical injection) [4]. A semiconductor laser on its own exhibits only simple dynamics: any perturbation of its steady state is damped out in an oscillatory behavior with a frequency corresponding to the so-called relaxation oscillation frequency. The degrees of freedom linked to external perturbations may, however, lead to highly complex nonlinear dynamics and bifurcations, such as period doubling, quasiperiodicity, or even chaotic regimes [5]. A fundamental understanding of the nonlinear dynamics of externally driven semiconductor lasers is a major issue in any applications where instabilities need to be avoided or controlled. On the other hand, laser instabilities may also be considered as useful to develop new, specific applications. For example, synchronized optical chaos in coupled lasers can be implemented in data encryption and secure communication systems [6–8]. High-frequency robust intensity oscillations generated with optical feedback from short external cavities may lead to all-optical sources of microwave signals [9–17]. Injection locking of a slave laser to a master laser is also commonly used to enhance the spectral stability and minimize the chirp of the laser [18–20].

Recently, the vertical-cavity surface-emitting laser (VCSEL) has emerged as a key semiconductor laser device for high-performance optical communication networks, owing to its numerous advantages such as a low threshold current, a single-longitudinal-mode operation, a circular output-beam profile, and wafer-scale integrability [21]. VCSELs have also received significant attention for their unique polarization properties: the emitted light is linearly polarized (LP) but unlike in edge-emitting lasers, its direction can vary from device to device and may not remain stable as we modify the operating conditions such as the temperature or the injection current. The polarization instability typically consists of a polarization switching between the two orthogonal LP modes [22]. New, interesting dynamics may then occur when this unique polarization degree of freedom in VCSELs interacts with an external degree of freedom such as that related to optical feedback, optical injection, or current modulation. Optical feedback, for example, may induce low-frequency fluctuations associated with polarization chaos [23–27], polarization self-modulation at very high frequencies [9,11–14], polarization mode hopping, and coherence resonance phenomena [28–31]. Period-doubling cascades and chaotic regimes have also been reported in gain-switched, directly modulated VCSELs, related to either transverse mode [32] or polarization mode competition [33].

However, studies of the influence of optical injection on the VCSEL polarization dynamics remain scarce. It has been shown that the polarization state of a VCSEL can be con-

*Electronic address: Marc.Sciamanna@supelec.fr
†Also at Institute of Solid State Physics, 72 Tzarigradsko Chaussee Blvd., 1784 Sofia, Bulgaria.

trolled and switched by optical injection with orthogonal polarization [34,35]. We shall call this configuration $OI_{\perp}$, in order to indicate that the injected field has its polarization orthogonal to that of the slave VCSEL. Polarization switching occurs through injection locking where both the wavelength and polarization of the slave VCSEL are locked to the injected master field. The switching is furthermore accompanied by a hysteresis feature which allows for generating a memory effect by modulating the bias current of the master laser [36]. Another laser configuration, which we call $OI_{\parallel}$, consists of an injected field with a polarization parallel to that of the slave VCSEL. In such a laser system, Li *et al.* have reported a stable injection locking within a very large detuning range [37]. Outside the locking range, several dynamical instabilities have been reported such as wave-mixing regimes [38] and relaxation oscillation undamping. These results are similar to those obtained in edge-emitting lasers but the single-longitudinal-mode characteristic of a VCSEL allows us to observe features that would otherwise be hidden by longitudinal-mode hopping dynamics in conventional edge-emitting lasers, e.g., injection locking with large detunings [37] and bistability near the locking boundary [39]. Further investigations on the $OI_{\parallel}$ configuration have shown that regions of polarization chaos can be observed for both positive and negative detunings [40]. In these chaotic regimes, the LP mode with the polarization orthogonal to that of the injected field is excited and emits in complete antiphase with respect to the other LP mode, such that the total intensity remains almost constant with time. Finally, several studies have reported on transverse mode dynamics in VCSELs with optical injection. When the VCSEL exhibits two transverse modes with orthogonal polarizations, the injection of external light with the appropriate detuning and injection strength allows one to select one mode and to suppress the other mode [41,42]. On the other hand, single-mode operation is not possible when the VCSEL exhibits two transverse modes with parallel polarizations [42,43]. In that last case, complex dynamical instabilities have been shown including combination of in-phase and antiphase mode dynamics and chaotic pulsing [43]. Finally, it is worth mentioning that an in-depth analysis of the optical injection dynamics of VCSELs is clearly motivated by a large number of applications. The phase locking of arrays of VCSELs to a master laser has been reported as an efficient technique to yield nearly diffraction-limited output beams with a high peak power [44]. The switching between polarization modes and/or different transverse modes induced by optical injection is interesting for applications in all-optical signal processing, e.g., as all-optical inverters [45]. Recent experiments on injection-locked 1.55 μm VCSELs have reported a significant chirp reduction in 2.5 Gb/s transmission experiments [46] and an interesting reduction of distortion in analog modulation [47]; hence important improvements in the performances of directly modulated VCSELs. Other interesting applications are in mind, such as the locking of an uncooled tunable VCSEL to a desired wavelength in order to relax the requirements for expensive wavelength lockers in dense-wavelength division multiplexed transmission systems [48,49].

In this paper, we analyze theoretically the polarization dynamics of a VCSEL subject to optical injection in the $OI_{\perp}$ configuration. As mentioned before, there have been only a few analyses of the polarization properties of VCSELs in this optical injection configuration. Previous experiments on the same laser system have only investigated the averaged intensities in the two orthogonal, LP modes of the slave VCSEL in conditions such that the increase of injected power leads to a polarization switching with injection locking, i.e., the slave VCSEL locks its frequency and polarization to that of the master laser [34]. Numerical simulations on a rate equation model have reproduced qualitatively well the polarization switching and its hysteresis feature [50]. However, to the best of our knowledge, the polarization dynamics in this route to polarization switching has never been investigated and the existence of possibly different scenarios for polarization switching has never been discussed. We unveil here interesting polarization behaviors as we increase the injection strength and as a function of the detuning between the slave VCSEL and the master laser. Different scenarios for polarization switching are investigated in detail through a mapping of the polarization dynamics in the plane of the injection parameters. While the free-running VCSEL exhibits a stationary x-LP mode, the increase of injected power typically leads first to complex multiwave-mixing dynamics with a combination of in-phase and antiphase intensity behaviors in the two LP modes. In-phase time-periodic, period-doubled, quasiperiodic, or even chaotic regimes are also found in the two LP modes in the route to the polarization switching. As a main result, we can point to the report of a stationary case for which the two LP modes are both locked to the master frequency. This case, which we call the elliptically polarized injection-locked (EPIL) state, therefore corresponds to a case for which the slave VCSEL locks in frequency to the master laser but still exhibits different polarization. The EPIL stationary dynamics may undergo a Hopf bifurcation leading to in-phase time-periodic intensity dynamics in the two LP modes. The limit cycle regime then progressively evolves to chaotic dynamics through a period-doubling cascade. Modern continuation techniques allow us to get insight into the existence and stability conditions of the EPIL steady state. An unfolding mechanism is shown as we vary the detuning and as a result, we find that the stability region of the EPIL solution is delimited by two codimension-2 Gavrilov-Guckenheimer bifurcations. These points are analyzed as a function of the laser parameters. Finally, we report on an additional case of bistability in injection-locked laser diodes for which the two-mode injection-locked solution (EPIL) coexists with the solution locked to the master polarization. Our results show that, by contrast to cases previously analyzed, the polarization switching does not necessarily occur through injection locking and, moreover, injection-locking situations may be found that are not accompanied by polarization switching. Our results are thought to be of interest not only for the fundamental understanding of the polarization properties in such a laser system but also for practical issues related to polarization control in VCSELs and fast polarization-switching mechanisms. They furthermore motivate additional experimental investigations.

We have organized our paper as follows. In Sec. II we introduce the model and its parameters. A route to polariza-

tion switching is analyzed in Sec. III for the experimental conditions of Pan *et al.* [34]. Section IV shows different dynamical scenarios, depending on the detuning between the slave VCSEL and the master laser. A mapping of the polarization dynamics in the injection-strength–detuning plane is unveiled. A more detailed stability analysis of the steady states is shown in Sec. V, with particular attention paid to the bifurcation boundaries of the EPIL state. Finally, we summarize our main conclusions in Sec. VI.

II. RATE EQUATION MODEL

Our model is based on the San Miguel, Feng, and Moloney (SFM) rate equations for a solitary VCSEL operating in the fundamental transverse mode regime [51]. These equations are the result of a semiclassical two-level Maxwell-Bloch approach applied to a scheme with four discrete energy levels. These energy levels are associated with two radiating transitions between conduction and valence bands, for which the respective carriers are of opposite spins. They are given by six real nonlinear and coupled differential equations for the two linearly polarized slowly varying components of the field $F_{x,y}$ and for two carrier variables D and d. D accounts for the total population inversion between conduction and valence bands, while d is the difference between population inversions for the spin-up and spin-down radiation channels.

We have extended the SFM model to account for the injection of an external field with a linear polarization orthogonal to that of the free-running VCSEL. In our simulations, the parameters of the model are chosen such that the free-running VCSEL exhibits a stable and stationary x-LP state. We therefore choose the optical injection along the y direction. The SFM model extended to y-LP optical injection and written in the frequency reference frame of the master laser is given by

$$\frac{dF_x}{dt} = \kappa(1+i\alpha)(DF_x + idF_y - F_x) - i(\gamma_p + \Delta\omega)F_x - \gamma_a F_x, \tag{1}$$

$$\frac{dF_y}{dt} = \kappa(1+i\alpha)(DF_y - idF_x - F_y) + i(\gamma_p - \Delta\omega)F_y + \gamma_a F_y + \kappa_{inj}E_{inj}^0, \tag{2}$$

$$\frac{dD}{dt} = -\gamma_e[D(1+|F_x|^2+|F_y|^2)] + \gamma_e\mu - i\gamma_e d(F_yF_x^* - F_xF_y^*), \tag{3}$$

$$\frac{dd}{dt} = -\gamma_s d - \gamma_e d(|F_x|^2+|F_y|^2) - i\gamma_e D(F_yF_x^* - F_xF_y^*). \tag{4}$$

The internal VCSEL parameters are as follows: κ is the field decay rate, γ_e is the decay rate of D, γ_s is the spin-flip relaxation rate (which accounts for the different microscopic mechanisms involved in the homogenization of the carrier spins), α is the linewidth enhancement factor, μ is the normalized injection current ($\mu=1$ at threshold), γ_a is the linear dichroism, and γ_p is the linear birefringence. κ_{inj}, E_{inj}^0, and $\Delta\omega$ are the optical injection parameters. κ_{inj} is the coupling coefficient, E_{inj}^0 is the injected field amplitude, and $\Delta\omega$ is the detuning between the master and slave frequencies. In our VCSEL problem the free-running laser may exhibit two frequencies, which correspond to the frequencies of the two linearly polarized modes. In the stationary case, the frequencies of the two LP modes are given by $\omega_{x,y} = \mp\gamma_p \pm \alpha\gamma_a$. Similarly to a previous numerical study of optical injection in VCSELs with the SFM model [50], we consider the frequency detuning as the detuning between the master frequency ω_{inj} and a frequency ω_{th} intermediate between that of the x- and the y-LP modes [$\omega_{th}=(\omega_x+\omega_y)/2$], i.e., $\Delta\omega=\omega_{inj}-\omega_{th}$.

III. ROUTE TO POLARIZATION SWITCHING

We have simulated the experimental configuration of Pan *et al.* [34], in which a free-running VCSEL that emits in the x-LP mode is subject to optical injection from a master laser with a y-LP polarization. The parameters of the SFM model are taken such that it reproduces the polarization characteristics of the solitary VCSEL as reported in this experiment. The reported frequency difference between the two orthogonal LP modes is about 9 GHz. Since the frequency difference between the two LP modes is approximately given by $2\gamma_p/(2\pi)$, we consider $\gamma_p=30$ rad/ns. The values of the parameters γ_a, α, and γ_s are taken such that the solitary VCSEL switches as in the experiment from the vertical direction (y) to the horizontal direction (x) for an injection current of about 20% above threshold ($\mu=1.2$). The polarization-switching behavior of VCSELs in the framework of the SFM model depends on the combination of γ_p, γ_a, α, and γ_s [50]. We have checked numerically that a polarization switching from the y-LP to the x-LP mode occurs at about $\mu=1.2$ if we consider the parameters $\gamma_a=0.5$ ns^{-1}, $\gamma_s=50$ ns^{-1}, and $\alpha=3$. The photon decay rate and the carrier relaxation rates are taken as $\kappa=300$ ns^{-1} and $\gamma_e=1$ ns^{-1}, which are typical values for a semiconductor laser. As in the experiment of Pan *et al.* [34], we fix the current at about 50% above threshold ($\mu=1.5$), i.e., after the polarization-switching point, such that the VCSEL emits only in the x-LP mode, that is, with an orthogonal polarization with respect to that of the injected field.

The coupling coefficient κ_{inj} multiplied by the injection amplitude E_{inj}^0 gives the injection strength per unit of time. This quantity is difficult to estimate from the experiment since it depends among other things on the quality of the alignment between the master and slave lasers. We will consider the parameter κ_{inj} fixed to $\kappa_{inj}=\kappa$, which corresponds to the optimal case of a mode-matched injected input beam [50]. Our bifurcation parameters are the frequency detuning $\Delta\omega$ and the amplitude of the injection E_{inj}^0.

We have first followed the experimental procedure of Pan *et al.* [34] to compute the polarization-resolved ouput power as a function of the injected optical power. The detuning has been fixed to $\Delta\omega=-\gamma_p=-30$ rad/ns, which means that the frequency of the master laser almost coincides with the fre-

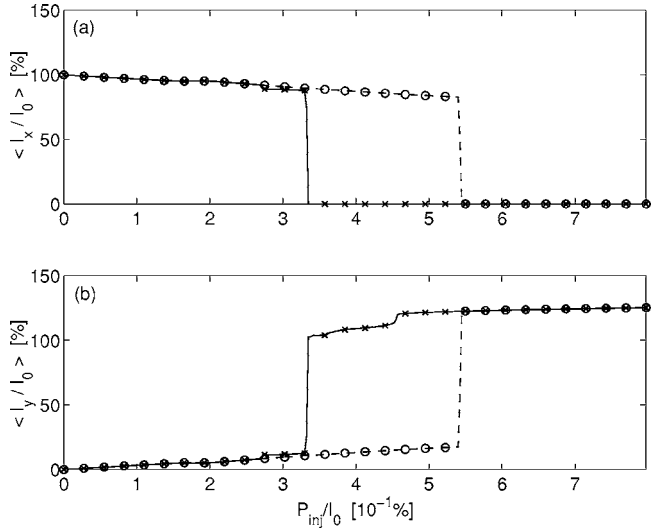

FIG. 1. Polarization switching occurring upon injection of a field with first linearly increasing and then linearly decreasing intensity. The LP mode intensities $I_{x,y}$ are plotted as a function of the injected power P_{inj}, in proportion of the free-running emitted power I_0. The intensities have been averaged over 80 ns. The dashed line with circles corresponds to the case of an increasing injected power, while the solid line with crosses corresponds to the case of a decreasing injected optical power.

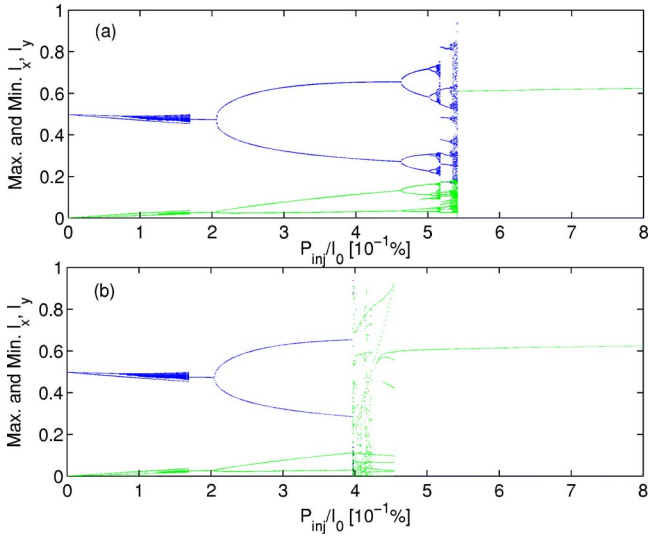

FIG. 2. (Color online) Bifurcation diagram of I_x (blue) and I_y (green) as a function of P_{inj}/I_0, for the same parameters as in Fig. 1 and for either increasing (a) or decreasing (b) injection strength.

quency of the free-running VCSEL when it emits in the x-LP mode. The injected optical power was increased linearly in time until polarization switching occurred, and then the injected optical power was decreased to zero. The SFM model extended to optical injection [Eqs. (1)–(4)] is integrated for each value of the injected optical power and the numerically computed intensities in the two LP modes $I_{x,y} \equiv |F_{x,y}|^2$ are averaged over 80 ns to account for the limited bandwidth of a slow photodetector, after letting the time for the transient to die off. For each value of P_{inj}/I_0, the initial conditions for the simulations are taken as the final solutions of the previous iteration in the injection strength. In agreement with the experimental results [34], we find a polarization switching with a region of bistability (hysteresis), as shown in Fig. 1. The LP mode intensities are plotted in Figs. 1(a) and 1(b), respectively, as a function of the injected optical power $P_{inj}=|E^0_{inj}|^2$. All intensities are normalized by the intensity of the free-running VCSEL $I_0 \equiv |F_x|^2+|F_y|^2$, where F_x and F_y are the LP components of the field in absence of optical injection. In our case I_0 is equal to the intensity of the x-LP mode in absence of optical injection, since the y-LP mode in the solitary VCSEL is nonlasing. Adiabatically sweeping the injected power from 0% to 0.8% of the emitted power I_0, we find a hysteresis cycle for both polarization components.

It is worth noting that a similar result has been obtained by Martin-Regalado *et al.* [50] using the same SFM model extended to optical injection except that the authors also extended the SFM model to account for the Gaussian transverse profile of the electric field instead of the plane-wave approximation of the SFM model. Our results indicate that this extension of the SFM model is not necessary to capture the features of the experimental results by Pan *et al.* [34].

Previous experimental results [34] and numerical simulations [50] have considered only the time-averaged optical powers. However, it is expected that the optical injection may induce a polarization dynamics in the VCSEL on a fast time scale, of the order of nanoseconds or even less [52]. These fluctuations of the polarization-resolved intensity have not been captured by the slow photodetector of the experimental setup in Ref. [34] and have not been investigated in the numerical analysis of Martin-Regalado *et al.* [50]. Our objective in this paper is then to investigate the polarization dynamics of the VCSEL in this route to switching induced by optical injection, first for parameters that are close to the experimental analysis of Pan *et al.* [34], and then for several combinations of frequency detuning $\Delta\omega$ and injected optical power P_{inj}.

Our first step in the analysis of the polarization dynamics is the computation of the bifurcation diagram of $I_{x,y}$ as a function of the normalized injected power P_{inj}/I_0. For each value of P_{inj}/I_0 we have numerically simulated the time traces of I_x and I_y and sampled the successive extrema of the LP mode intensities. These extrema are plotted on the vertical axis. This procedure is repeated for each value of P_{inj}/I_0, by taking as initial conditions for the simulations the final solutions of the previous iteration in the bifurcation parameter. The parameters are identical to those used to compute the hysteresis cycle of Fig. 1, hence allowing a direct comparison between the averaged procedure and the dynamical analysis. The bifurcation diagram is plotted in Fig. 2. The x-LP and y-LP mode intensities are plotted for either an increasing (a) or a decreasing (b) injection strength.

As shown in Fig. 2, the route to polarization switching induced by optical injection corresponds to a cascade of bifurcations to qualitatively different dynamical behaviors including stationary, time-periodic, quasiperiodic, and chaotic regimes. The comparison between Figs. 2(a) and 2(b) shows furthermore that a solution which is locked to the master laser polarization and frequency (at large injection strength) may coexist in a quite large range of injection strength (between $P_{inj}/I_0 \sim 0.4\%$ and $\sim 0.53\%$) with time-periodic,

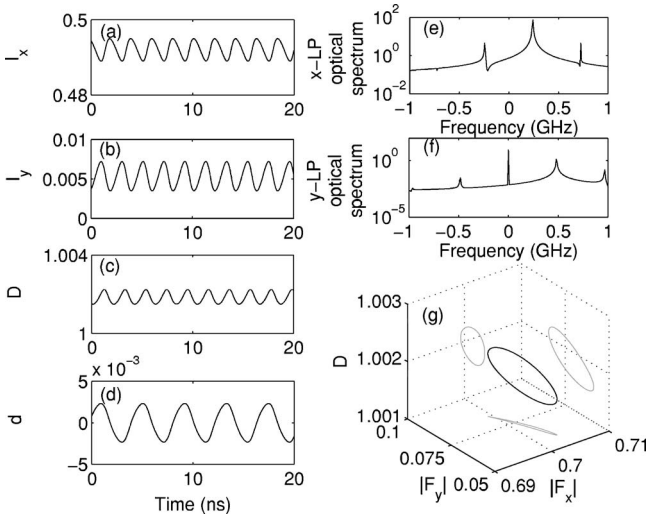

FIG. 3. Polarization dynamics resulting from wave mixing for a small injection amplitude. (a) and (b) show the intensities of the two LP modes, $I_{x,y}$, respectively. (c) and (d) show time traces of the two carrier variables D and d. The optical spectra of the two LP modes are shown in (e) and (f). A three-dimensional projection of the system trajectory is shown in (g), in the space $(|F_x|,|F_y|,D)$. The injection amplitude is fixed at $P_{inj}/I_0=0.03\%$, and the other parameters are as in Fig. 2.

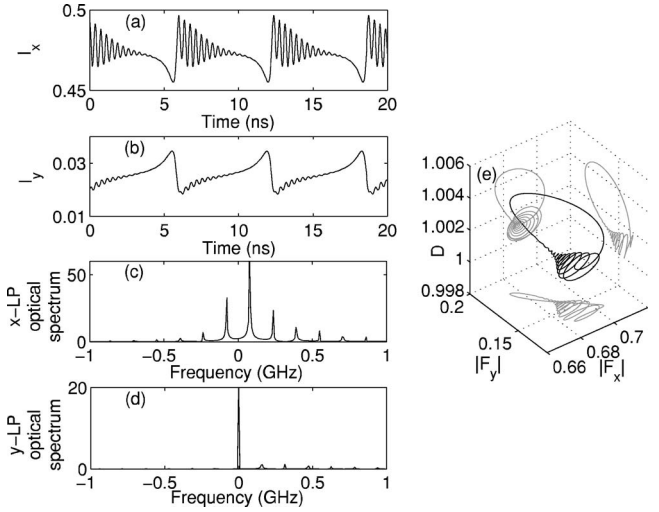

FIG. 4. As in Fig. 3 but illustrating multiwave-mixing dynamics and combination of in-phase–antiphase polarization dynamics. The injection strength is taken as $P_{inj}/I_0=0.16\%$.

period-doubled, or even chaotic regimes. These time-periodic and more complex dynamics originate from another steady-state solution located at smaller values of the injected power. This second steady-state solution corresponds to another injection-locking mechanism, as will be detailed in the following. We shall decribe these dynamics and the locking mechanisms in the following subsections, on the basis of time traces and optical spectra in the two LP modes.

A. Wave-mixing dynamics and frequency pulling

As we increase the injected power from zero, the bifurcation diagram of Fig. 2 shows that the optical power in the depressed y-LP component of the slave VCSEL increases and the intensities in the two LP modes exhibit a small time-periodic modulation with several different but close extrema. The intensities of the two LP modes exhibit a time-periodic dynamics that consists of a very small modulation of the output power; see Figs. 3(a) and 3(b). The time evolution of the carrier variables D and d is shown in Figs. 3(c) and 3(d). The optical spectra of the two LP modes are plotted in Figs. 3(e) and 3(f). In Fig. 3(g) is shown a projection of the system trajectory in the three-dimensional phase space $(|F_x|,|F_x|,D)$, while the complete phase space is of dimension 6.

The LP mode intensities are slightly modulated and the modulation frequency almost corresponds to 0.4 GHz. This frequency is much smaller than the relaxation oscillation frequency of the free-running VCSEL $[\omega_{RO}/(2\pi) \equiv \sqrt{2\kappa\gamma_e(\mu-1)} \simeq 2.77$ GHz] or the beating frequency between the two LP modes $[2\gamma_p/(2\pi) \simeq 9.5$ GHz]. An analysis of the optical spectra in Figs. 3(e) and 3(f) shows that the x-LP mode exhibits a dominant peak at a frequency almost corresponding to the frequency of the free-running VCSEL in the x-LP state, but slightly shifted by optical injection. The master frequency corresponds to zero since we operate in the reference frame of the master laser. The frequency of the free-running VCSEL in the x-LP state is shifted from the master frequency by $f_{\text{off}} \simeq \alpha\gamma_a/(2\pi)=0.24$ GHz. Much weaker side peaks appear, which are approximately separated from the dominant peak by about $2f_{\text{off}}$. On the other hand, the spectrum of the y-LP mode exhibits a dominant peak at the master frequency (0). This dominant peak is however much weaker than the dominant peak in the x-LP mode. Side peaks also appear, which are separated from the master frequency by a multiple of $2f_{\text{off}}$. In summary, the spectrum of the total intensity exhibits a dominant peak at the slave laser frequency (f_{off} in the reference frame of the master laser), a weaker peak at the master frequency (0), and side peaks which are separated from the slave frequency by multiples of f_{off}. A beating occurs between the slave frequency and the master frequency, which are separated by f_{off}. The beating results in a pulsation of the population inversion, which then yields an intensity modulation in the two linearly polarized components of the VCSEL. Since in the SFM model two carrier reservoirs with opposite spins are defined, the pulsation of the carrier population must be analyzed through the time dependency of the two carrier variables D and d, as shown in Figs. 3(c) and 3(d). Interestingly, the variable D oscillates with a frequency of about $2f_{\text{off}}$ while the d variable oscillates with a frequency twice smaller, i.e., f_{off}. While we can identify the mechanism responsible for the intensity oscillations as a wave mixing (since a beating occurs at a frequency that results from the interaction between the slave and master fields), a complete description of this wave-mixing mechanism would require an in-depth analytical study of the perturbed SFM model in presence of injection, which is left for future work.

More complex wave-mixing processes and higher harmonics may be observed when increasing the injection amplitude, as shown in Fig. 4. The intensities of the two LP modes still exhibit a slow time-periodic dynamics but now

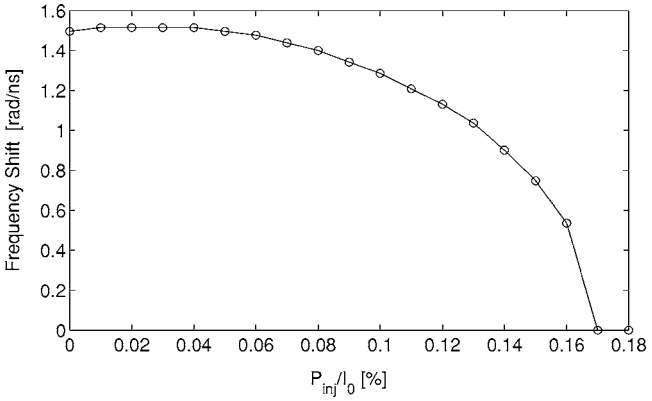

FIG. 5. Frequency pulling in the wave-mixing dynamics. The frequency shift of the dominant peak in the x-LP mode optical spectrum is measured in units of angular frequencies in the reference frame of the master frequency, and as a function of the injected power P_{inj}/I_0. The parameters are the same as in Fig. 2. The frequency of the dominant peak shifts in the direction of the master frequency as we increase the injection strength and locks to the master frequency for a sufficiently large injected power.

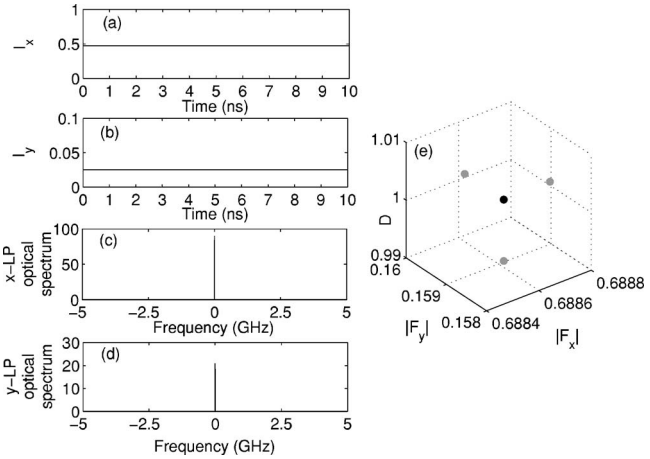

FIG. 6. As in Fig. 3 but illustrating an elliptically polarized injection-locked steady state. The injection amplitude is taken as $P_{inj}/I_0=0.18\%$.

the LP modes relax with faster oscillations at the frequency of the relaxation oscillation. Interestingly, the two LP modes exhibit a combination of in-phase and antiphase pulsating dynamics, i.e., the two LP modes are anticorrelated at the time scale of the slow oscillations and they exhibit an in-phase dynamics at the fast time scale of the relaxation oscillations. This in-phase–antiphase combination appears to be a generic feature of polarization dynamics in VCSELs with additional degrees of freedom: it has been found also in polarization dynamics induced by optical feedback [24–27] and in gain-switched VCSELs [33]. In our optical injection system, the in-phase dynamics occurs at the time scale of the relaxation oscillation period (0.36 ns) while the antiphase dynamics occurs at the much slower time scale of the beating between the master and the slave fields.

The wave-mixing dynamics occurs in the route to the VCSEL injection locking and is accompanied by a modulation of the laser intensity and by side peaks in the optical spectra. Another characteristic of this wave-mixing dynamics is the frequency pulling. In absence of optical injection, the optical spectrum consists of a single peak located at the angular frequency $\alpha\gamma_a=1.5$ rad/ns with respect to the angular frequency corresponding to the master laser, i.e., in the frequency reference frame of the master laser. This peak corresponds to the frequency of the x-LP mode since the y-LP mode is not lasing in the free-running VCSEL. As we increase the injected power, side peaks complement this dominant peak in the x-LP mode optical spectrum but moreover the dominant peak progressively shifts in the direction of the master frequency, as indicated in Fig. 5. As the injection strength increases the slave laser is first slightly pushed away from the master laser and then strongly pulled toward the master frequency. For a sufficiently large injected power P_{inj}/I_0 (here close to $P_{inj}/I_0\simeq 0.19\%$), the VCSEL exhibits an injection locking (to an elliptically polarized injection-locked state; see below) and the frequency shift with respect to the master frequency therefore goes to zero, since the slave VCSEL is locked to the frequency of the master laser. Analytical approximations for the dependency of the frequency shift on the injection strength and detuning have been reported in the case of a single-mode edge-emitting laser subject to weak optical injection [53], but similar results are not available for our two-mode VCSEL problem.

B. Injection-locked states and time-periodic, complex polarization dynamics

For a slightly larger amount of optical injection, the intensities of the two LP modes now exhibit a stationary behavior, i.e., they remain constant in time. This region of stationary state with $I_x\neq I_y\neq 0$ is found only in a small region of injected optical power. This dynamics is detailed in Fig. 6, in which the time traces of the LP mode intensities ($I_{x,y}$) are plotted in Figs. 6(a) and 6(b) together with the corresponding optical spectra in Figs. 6(c) and 6(d), respectively. The LP mode intensities are steady and this steady-state operation of the VCSEL corresponds to an injection locking in the sense that the slave laser optical frequency is locked to that of the master laser. In our VCSEL problem, the free-running frequency is in fact made of two slightly shifted frequency components that correspond to the frequencies of the two LP modes shifted as a result of birefringence effects. The injection-locked state of Fig. 6 corresponds to a case of injection locking in which both frequency components are locked to the frequency of the master laser. Since the two LP modes do not necessarily exhibit the same intensities and phases, this case corresponds to an *elliptically polarized injection locked* steady state. The system trajectory obviously corresponds to a fixed point with nonzero intensities in any of the two LP mode intensities, as shown in Fig. 6(e).

This case of injection locking arises from the interaction between the polarization mode competition in VCSELs and the optical injection effects. As we will show in Sec. V, the existence of a stable EPIL is strongly dependent on the value of the frequency detuning and injected optical power.

As shown in the bifurcation diagram of Fig. 2, the EPIL steady state destabilizes with a Hopf bifurcation for a larger

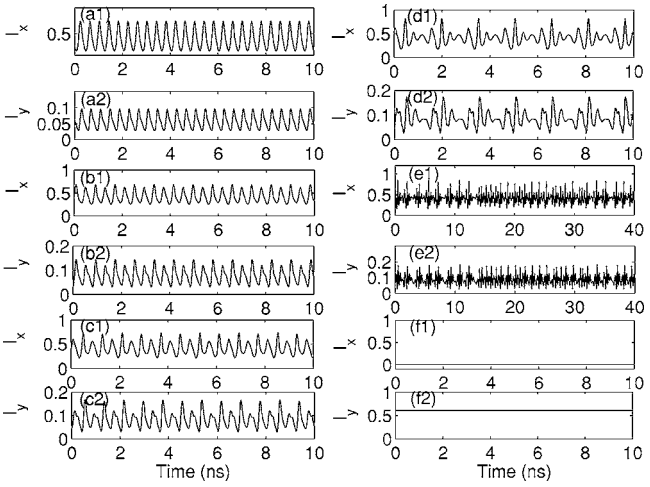

FIG. 7. Time traces of the LP mode intensities $I_{x,y}$ for increasing values of the injected power: P_{inj}/I_0= (a1),(a2) 0.35%, (b1),(b2) 0.47%, (c1),(c2) 0.51%, (d1),(d2) 0.53%, (e1),(e2) 0.54%, and (f1),(f2) 0.55%.

amount of injection amplitude. The resulting time-periodic dynamics then exhibits a cascade of period-doubling bifurcations to more complex, chaotic regimes. This cascade of bifurcations on limit cycle solutions is analyzed in more detail in Figs. 7 and 8. Figure 7 shows the time traces of I_x and I_y for increasing values of the injection strength. The corresponding optical spectra are plotted in Fig. 8.

The Hopf bifurcation on the EPIL steady state leads to a time periodic intensity modulation in the two LP mode intensities; see Figs. 7(a1) and 7(a2). The x-LP mode is the dominant mode (the one with the largest intensity) but both LP modes oscillate with the same frequency, which is close to the relaxation oscillation frequency of the free-running VCSEL (about 2.5 GHz). Interestingly, the two LP modes oscillate in phase in this time-periodic dynamics that emerges from a Hopf bifurcation, in contrast to the antiphase

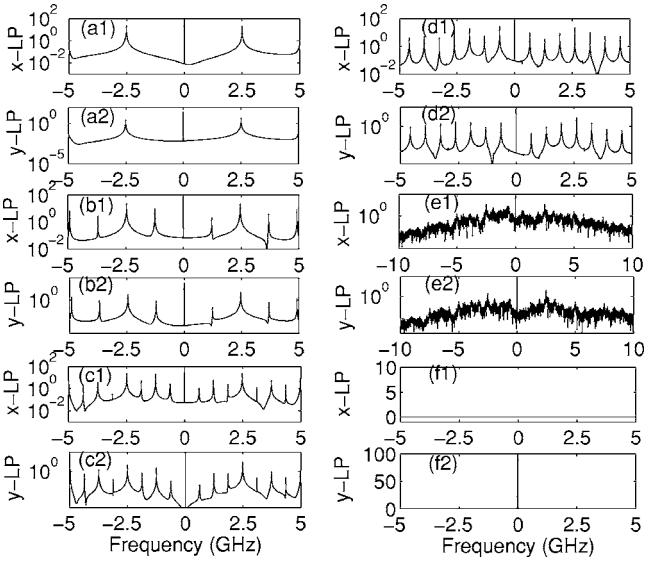

FIG. 8. Optical spectra of the x- and y-LP modes corresponding to the polarization dynamics of Fig. 7.

oscillations that are observed in the time-periodic dynamics resulting from wave mixing (see Fig. 3). The polarization-resolved optical spectra shown in Figs. 8(a1) and 8(a2) are also very different from the ones shown in Fig. 3 for the wave-mixing dynamics: now the dominant peak in the two LP modes is located at the frequency of the master laser and symmetric side peaks appear, which are separated from the dominant peak by multiples of the oscillation frequency (about 2.5 GHz).

As we still increase the injected power further, the time-periodic dynamics in the two LP modes may undergo a secondary period-doubling bifurcation, as shown in Figs. 7(b1), 7(b2), 8(b1), and 8(b2). The two LP mode intensities still oscillate with a fundamental frequency close to 2.5 GHz but now the intensities are also modulated on a smaller frequency which corresponds to half of the fundamental frequency. This period doubling is also observed in the polarization-resolved optical spectra. The dominant peak is still located at the frequency of the master laser and the strongest side peaks are still located at multiples of the fundamental oscillation frequency (2.5 GHz). However, new side peaks also appear at multiples of 1.25 GHz, i.e., half of the fundamental frequency.

The period-doubling cascade continues as we increase the injection amplitude further, leading to a period-4 time-periodic dynamics in the two LP modes; see Figs. 7(c1), 7(c2), 8(c1), and 8(c2). Two LP mode intensities exhibit four different extrema within each period. The time traces of LP mode intensities exhibit a period equal to about 1.6 ns, i.e., twice larger than the 0.8 ns period of the period-2 oscillation shown in Figs. 7(b1) and 7(b2), but the intensities still oscillate with the fundamental frequency of 2.5 GHz (an oscillation at each 0.4 ns). The polarization-resolved optical spectra exhibit new side peaks that are located at multiples of one-fourth of the fundamental frequency (0.75 GHz).

For a slightly larger amount of injected optical power, the period-4 dynamics in the two LP modes exhibits very different quantitative features than the ones analyzed in Figs. 7(c1), 7(c2), 8(c1), and 8(c2). This different period-4 dynamics is detailed in the cases Figs. 7(d1), 7(d2), 8(d1), and 8(d2). The two LP mode intensities still exhibit a period of about 1.6 ns and oscillate at each period corresponding to the fundamental frequency (0.4 ns), but the intensity oscillations with a high frequency are more pronounced than for the previously analyzed period-4 dynamics. The LP mode intensities span a wider range of intensities than shown in Figs. 7(c1) and 7(c2). The polarization-resolved optical spectra exhibit the same features as for the period-4 dynamics shown in Figs. 8(c1) and 8(c2) but the side peaks located at multiples of 0.75 GHz are much stronger than for the previously reported period-4 dynamics.

A cascade of period-doubling bifurcations then accompanies the polarization switching induced by optical injection. In a small region of optically injected power, very close to the one that leads to the polarization switching, the polarization dynamics becomes very complex, as shown in Figs. 7(e1) and 7(e2). The LP mode intensities do not exhibit a clear periodicity but instead resemble irregular bursts of power that extend over a wide range of intensity values. The polarization-resolved optical spectra plotted are extremely

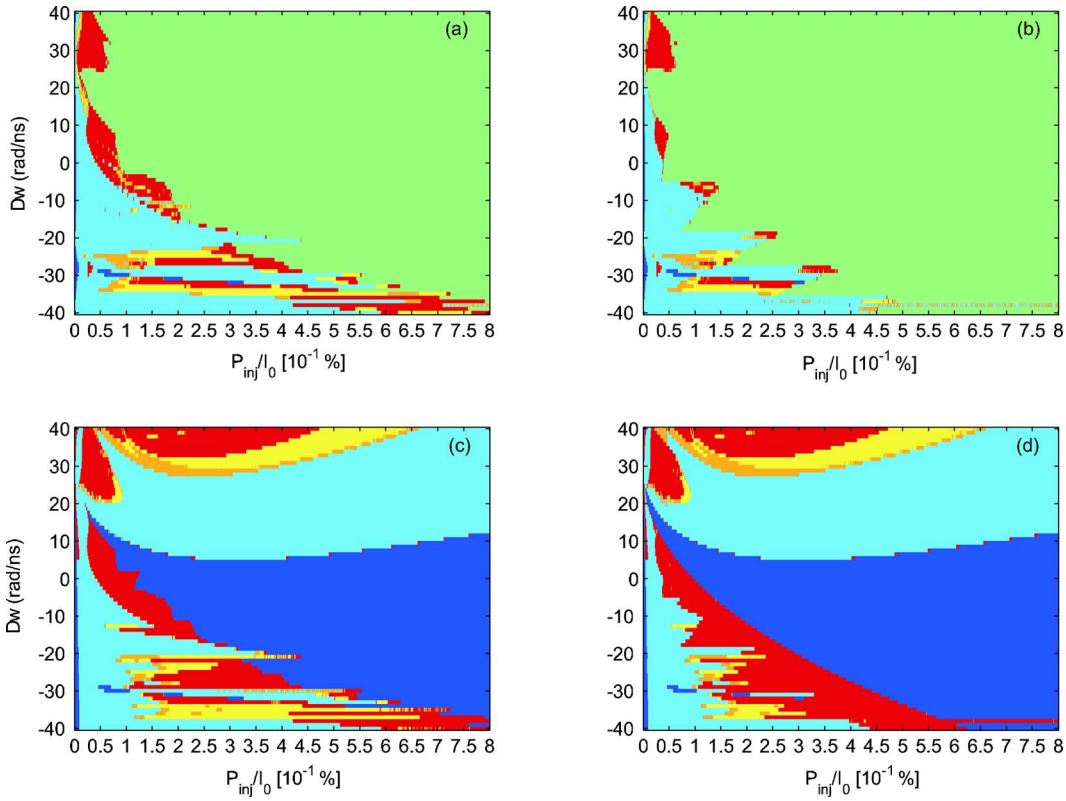

FIG. 9. (Color online) Mapping of the polarization dynamics in the plane of the injection parameters $(\Delta\omega, P_{inj}/I_0)$. Each point in the mapping is associated with a color, the colors being related to the number of extrema in the intensity time traces as specified in the text. The other laser parameters are the same as in Fig. 2.

broad and continuous, with a dominant peak located at the frequency of the master laser but without any discrete structure of peaks. The laser system therefore exhibits features that correspond to a chaotic dynamics resulting from a cascade of period doubling bifurcations.

Finally, for large values of the injected power, the bifurcation cascade leads to a polarization switching induced by optical injection. The polarization switching corresponds to a switch-off of the x-LP mode and an injection locking of the y-LP mode, as analyzed in Figs. 7(f1), 7(f2), 8(f1), and 8(f2). The y-LP mode exhibits a steady intensity while the x-LP mode is completely depressed. The optical spectrum of the y-LP mode exhibits a single peak located at the frequency of the master laser, hence corresponding to an injection-locking mechanism. The slave VCSEL laser is injection locked to the master laser but moreover, and by contrast to Fig. 6, its polarization is now locked to the polarization of the master laser.

IV. MAPPING OF POLARIZATION DYNAMICS

In Sec. III, we have analyzed the VCSEL polarization dynamics in the case of a detuning $\Delta\omega=-\gamma_p=-30$ rad/ns, i.e., such that the frequency of the master laser is very close to the frequency of the free-running VCSEL when it emits in the x-LP mode. The route to the polarization switching induced by optical injection was shown to involve a bifurcation cascade with steady states, and time-periodic and more complex or chaotic dynamics. Of particular interest is the existence of a two-mode injection-locking steady state, for which the two polarization modes both lock to the master laser. One may expect that the polarization dynamics and this two-mode injection-locking regime are strongly dependent on the detuning $\Delta\omega$. Our results therefore motivate a detailed mapping of the polarization dynamics in the plane of the injection parameters, i.e., $(P_{inj}/I_0, \Delta\omega)$.

The mapping of polarization dynamics is shown in Fig. 9 (enlargements of the region of EPIL steady-states are also shown in Fig. 10). Four mappings are shown. The two mappings in the left (right) column show the dynamics of the x-LP mode (a) [(b)] and the y-LP mode (c) [(d)] when the injection amplitude is adiabatically increased (decreased).

We have defined 200 uniformly distributed values of the detuning and 800 uniformly distributed values of the injection amplitude. For each pair of detuning and injection amplitude, we have numerically computed the extrema of the LP mode intensities as a function of time. We have then classified the dynamics according to the complexity of the polarized intensity time traces, i.e., according to the number of different successive extrema. The qualitatively different dynamics are associated with different colors in the mapping of Fig.9 (color online only). A dark blue color is used whenever the LP mode intensity is steady as function of time (only one extremum). The light blue, orange, and yellow colors correspond to qualitatively different time-periodic dynamics, in which the intensity time trace exhibits two, three, or four different extrema, respectively. Examples of time-periodic

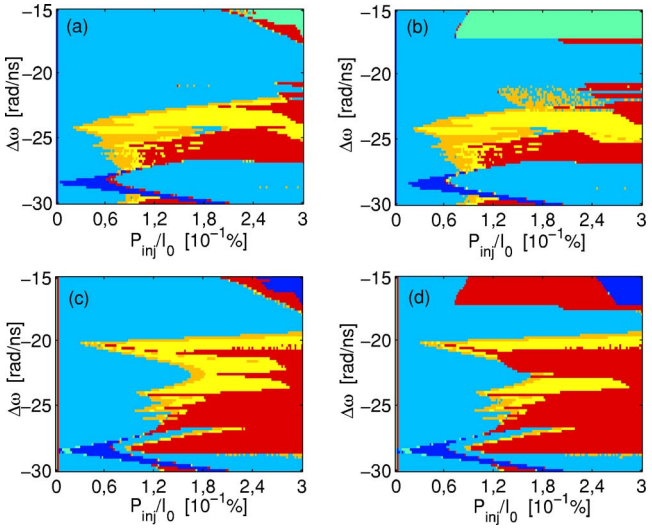

FIG. 10. (Color online) Zoom of the mapping of the polarization dynamics in the plane of the injection parameters $(\Delta\omega, P_{inj}/I_0)$, in order to better analyze the region of steady states (in dark blue) corresponding to elliptically polarized injection-locked states.

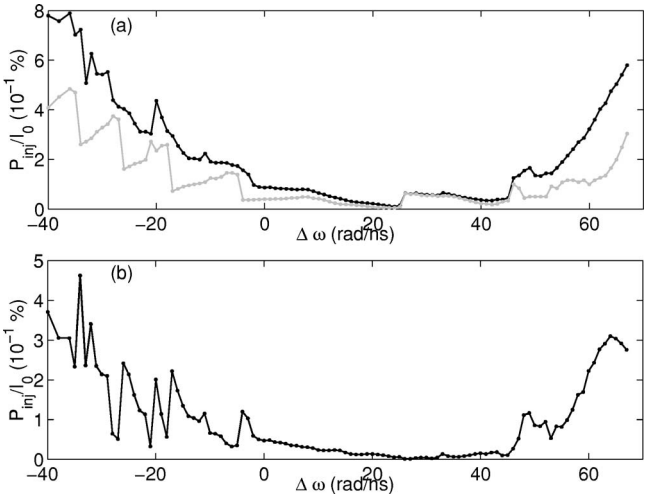

FIG. 11. (a) Injection strength at which occurs a polarization switching to the y-LP mode. Switch-off power levels for increasing injected power and switch-on power levels for decreasing injected power are plotted in black and gray, respectively, as a function of the detuning $\Delta\omega$. The hysteresis size is plotted in (b) as a function of the detuning.

dynamics associated with the light blue color are those shown in Figs. 3(a) and 3(b), 7(a1), and 7(a2). The yellow color is typically used for a period-doubling regime such as that plotted in Figs. 7(b1) and 7(b2). We use the red color when the number of different extrema exceeds 4, which we identify as a complex laser dynamics, possibly chaotic. Finally, the green color is used when the intensity of one of the two LP modes is zero. In our VCSEL configuration, this can only be the case for the x-LP mode once optical injection has induced a polarization switching to the y-LP mode.

The boundary between areas with different colors can be identified as a bifurcation, in the sense that the dynamics changes qualitatively if one sweeps the parameters across this boundary. Some important conclusions can be drawn from the mapping, regarding the regions of injection locking, the dependency of the polarization-switching boundary on the detuning, and the multistability between several attractors.

We find two regions of injection-locking steady states. The first, largest injection-locking area (in dark blue) corresponds to the slave laser being locked in frequency and polarization to the master laser. The y-LP mode of the slave VCSEL is then in a locked steady-state at the frequency of the master laser, while the x-LP mode is depressed. This region of injection locking spans a large range of injection amplitude and detuning and extends much more in the negative detuning side. It resembles very much the one found in single-mode edge-emitting lasers subject to optical injection (see, e.g., Refs. [54,55]). The stability of this injection-locked steady state is delimited by two bifurcations. The large injection strength bifurcation corresponds to a Hopf bifurcation to a time-periodic dynamics (light blue color). The smaller injection strength bifurcation is a saddle-node bifurcation, at which are created a node (the stable injection-locked steady state) and a saddle. A second region of injection-locked state corresponds to a two-mode injection locking, i.e., the two LP modes are both locked to the master laser and the laser emits an elliptically polarized injection-locked steady state. This region is found only in a small range of injection parameters, for $\Delta\omega \simeq -30$ rad/ns and small values of the injection strength. A zoom of the mapping is shown in Fig. 10, in order to better analyze the stability boundaries of this region of EPIL steady state. The bifurcation boundary at larger injection strength corresponds to a Hopf bifurcation, leading to time-periodic dynamics in the two LP modes which may further evolve to a period-doubling route to chaos. Our mapping suggests that the bifurcation located on the small injected power side corresponds to a saddle-node bifurcation. More detailed and systematic investigations of the stability of the EPIL steady state will be reported in Sec. V and will unveil a complete picture of the bifurcation lines.

The large green area for the mapping of the x-LP mode in Figs. 9(a) and 9(b) gives the polarization-switching boundary in the laser system. The polarization switching may be accompanied by an injection locking to the master frequency (as is the case for mostly negative detuning when crossing the dark blue region of the y-LP injection-locked state) but this is not necessarily the case: the switching occurring for a large positive detuning leads to a time-periodic or more complex dynamics in the y-LP mode but not to an injection locking. Very often the intensity dynamics close to the polarization-switching point is complex in the two LP modes, as indicated by the regions with red color close to the green switching boundary. Moreover, the hysteresis in the polarization switching is also unveiled in our mappings. For clarity, we have plotted in Fig. 11(a) the injection strength at which the y-LP polarization mode switches on (black) and off (gray), and in Fig. 11(b) the size of the hysteresis, as a function of the detuning. In agreement with the experiments of Pan *et al.* [34], the minimum injected power needed for polarization switching is found for detuning values $\Delta\omega \simeq \omega_y = \gamma_p - \alpha\gamma_a$, i.e., when the master laser frequency is

close to the frequency of the depressed free-running y-LP mode. Still in agreement with the reports of Pan *et al.* [34], there is a tendency for an increase of the hysteresis size as the master laser frequency moves away from ω_y. However, our extensive numerical simulations also show additional features, not observed in the previous experiments. We observe quite large fluctuations of the hysteresis size when the detuning is negative and more specifically in parameter regions where the switching is accompanied by injection locking to the y-LP mode. The hysteresis size increases in a much smoother way on the positive detuning side. While the overall tendency is an increase of the hysteresis size as $\Delta\omega$ differs from ω_y, there are also some ranges of detuning values for which the slope is opposite.

Another conclusion from the mapping is that the optically injected VCSEL exhibits several examples of multistabilities, i.e., coexistence of attractors for the same set of parameters. These multistable regimes are clearly unveiled if we compare the mappings for increasing and decreasing injection amplitudes, i.e., Figs. 9(a) and 9(c) versus 9(b) and 9(d). Bistability often occurs between a time-periodic dynamics and a complex or possibly chaotic dynamics as we approach the polarization-switching point. As shown in the bifurcation diagram of Fig. 2, there might be coexistence between the y-LP injection locked solution and a time-periodic, period-doubled or even chaotic dynamics emerging from the EPIL solution. The bistability and coexistence of attractors is more significantly pronounced for the negative detunings than for the positive detunings.

As already mentioned, the dynamics which are observed after the polarization switching point, i.e., once the VCSEL only emits in the y-LP mode, are similar to those found in single-mode edge-emitting lasers subject to optical injection [54,55]; see, e.g., the region of stability for the y-LP injection-locked solution, the bubble of chaos for large positive detunings, and the unlocking transition to time-periodic dynamics for large values of the injection strength. However, several other dynamics appear in our two-mode VCSEL problem in the transition to the polarization switching, such as wave-mixing dynamics with two-mode competition, the EPIL solution and its destabilization through Hopf bifurcation, and also new bubbles of chaos with two-mode dynamics.

Increasing the γ_s parameter does not modify the y-LP injection locking area in the mapping of Figs. 9 and 10, as also explained in Sec. V. However, the area in the mapping corresponding to a stable EPIL solution may significantly shrink as γ_s increases. We analyze the underlying bifurcation mechanism in Sec. V; see Fig. 17. As for the more complex dynamics, we find numerically that increasing γ_s up to about 300 ns^{-1} (1) does not modify the areas corresponding to a period-doubling route to chaos in one or in the two polarization modes and which are observed for positive detuning values in Fig. 9, and (2) does not modify the polarization-switching boundary in the frequency detuning vs injection strength mapping. However, it is worth mentioning that increasing γ_s leads to a progressive shrinking of the areas in the mapping that correspond to wave mixing in the two polarization modes (dynamics as reported in Figs. 3 and 4) [16]. The two-polarization-mode wave-mixing dynamics

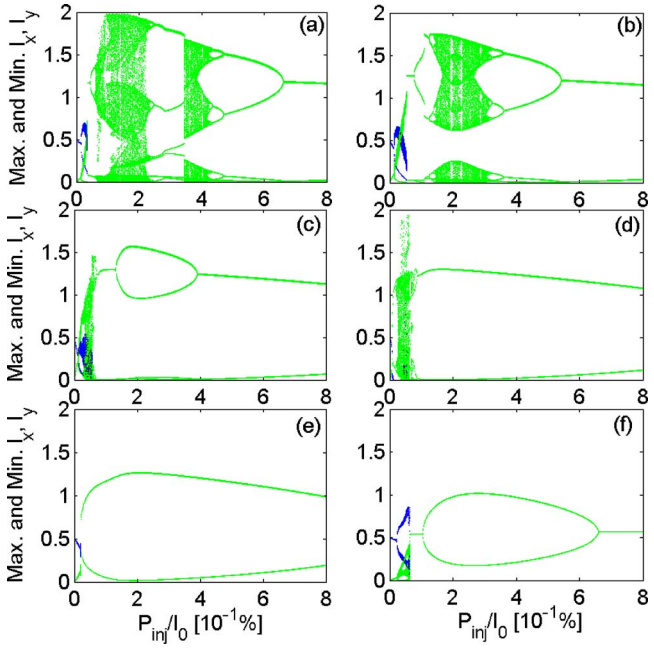

FIG. 12. (Color online) Bifurcation diagrams of the LP mode intensities as a function of the normalized injected power, for different positive values of the detuning $\Delta\omega$ and the same values of parameters as in Fig. 2: $\Delta\omega$= (a) 40, (b) 35, (c) 30, (d) 25, (e) 20, and (f) 10 rad/ns. The successive extrema of I_x (I_y) are plotted in black (gray) as we increase P_{inj}/I_0, which is our bifurcation parameter.

which occur in the route to polarization switching with injection locking are therefore strongly related to the strength of the nonlinear coupling process between the two orthogonal polarization modes.

The mapping shown in Fig. 9 summarizes the polarization dynamics in a large range of injection parameters but, on the other hand, the red color does not discriminate between extremely complex intensity dynamics such as chaotic regimes and time-periodic dynamics with a large number of different extrema or even quasiperiodic regimes. Locked time-periodic solutions in between chaotic solutions are also not plotted. In order to obtain more information on the detailed polarization dynamics, it is therefore important to complement the mappings with the computation of bifurcation diagrams for different sets of injection parameters.

Figure 12 plots the bifurcation diagrams of I_x and I_y as a function of the normalized injected power and for different values of positive detuning $\Delta\omega$, ranging from $\Delta\omega$=40 (a) to 10 rad/ns (f). As shown in the mapping of Fig. 9, the polarization dynamics for large positive detunings is characterized by the existence of two bubbles of chaos at small or moderate values of the injection amplitude. One of these chaotic regions occurs very close to the polarization-switching boundary and is characterized by complex dynamics in the intensities of the two LP modes. The second, larger region of chaos in the laser is found after the switching point and thus only the y-LP mode is lasing. The laser dynamics then bifurcates to simpler time-periodic oscillations as we increase the injection amplitude.

In Fig. 12(a), the x-LP mode gradually evolves from a slightly modulated intensity to a more complex dynamics as

we approach the value of injected power leading to the polarization switching. After the polarization switching occurs ($P_{inj}/I_0 \simeq 0.03\%$), the y-LP mode is the only lasing mode and exhibits a complex chaotic dynamics in a relatively large range of injected powers, as also shown by the red color in the mapping of Fig. 9. The bifurcation diagram shows that a locking to a time-periodic dynamics may occur between two regions of chaos (around $P_{inj}/I_0 \simeq 0.3\%$). This was not unveiled in the mapping since we have considered the same color for any intensity dynamics that exhibits more than four different extrema. It also justifies the need to complement the mapping of polarization dynamics by detailed bifurcation diagrams. An inverse period doubling cascade leads to a period-1 limit cycle oscillation in the y-LP mode for a large value of the injected power. The polarization dynamics in Fig. 12(b) is qualitatively similar to that shown in Fig. 12(a) but for a slightly larger value of the detuning.

The boundary of the bubble of chaos with only the y-LP mode lasing is progressively reached as we decrease $\Delta\omega$ to about 30 rad/ns; see Fig. 12(c) in which the y-LP mode exhibits a period-1 limit cycle oscillation in a large range of injection amplitude. The period-1 dynamics bifurcates to a period-doubling regime for $P_{inj}/I_0 \simeq 0.15\%$ but a reverse period doubling leads back to the period-1 time-periodic dynamics. For a still smaller value of the detuning [Fig. 12(d)], the y-LP mode exhibits a period-1 limit cycle oscillation for all values of injected optical powers after the polarization switching occurs. Before the polarization switching point, the x- and y-LP modes still compete with a chaoticlike dynamics with almost equal averaged intensities in the two LP modes (this dynamics corresponds to the second, small bubble of chaos shown in the mapping of Fig. 9 for positive detunings and small values of the injected amplitude). The boundary of this bubble is reached for about $\Delta\omega = 20$ rad/ns, as shown in Fig. 12(e). The route to polarization switching induced by optical injection then occurs through a simple time-periodic dynamics in the two LP modes, while after the switching occurs the y-LP mode keeps on exhibiting a period-1 time-periodic intensity in the range of injected power we investigate. Finally, in Fig. 12(f) is shown the situation for which an increase of injected power leads to a crossing of the Hopf bifurcation boundary of the injection locking region (the large dark blue region in the mapping of Fig. 9). As we increase the injected amplitude, the x-LP mode switches off and the y-LP mode is locked to the master laser. This injection-locking steady state destabilizes with a Hopf bifurcation for a slightly larger value of injected amplitude, which leads to a time-periodic dynamics. The injection-locking steady state restabilizes through a second supercritical Hopf bifurcation for $P_{inj}/I_0 \simeq 0.65\%$.

A second set of bifurcation diagrams is plotted in Fig. 13 for values of the detuning close to zero or negative. As also shown in the mapping of Fig. 9 and in the bifurcation diagram of Fig. 2, the route to polarization switching induced by optical injection for negative detunings is usually accompanied by either time-periodic or complex polarization dynamics, and possibly EPIL steady states. In the range of detunings $-20 < \Delta\omega < -15$ rad/ns, the switching induced by injection occurs through simple polarization dynamics, as shown in Fig. 13(a). The polarization modes exhibit

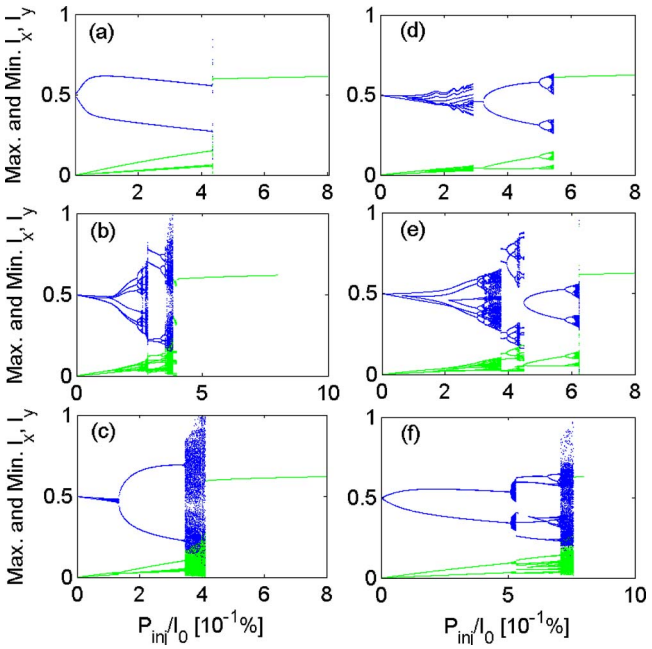

FIG. 13. (Color online) Bifurcation diagrams of the LP mode intensities as a function of the normalized injected power, for different values of the detuning $\Delta\omega$ and the same values of parameters as in Fig. 2: $\Delta\omega$= (a) −20, (b) −25, (c) −27, (d) −31, (e) −32, and (f) −39 rad/ns. The successive extrema of I_x (I_y) are plotted in black (gray) as we increase P_{inj}/I_0, which is our bifurcation parameter.

period-1 time-periodic behaviors before the polarization switching point and after the switching point, injection locking in the y-LP mode occurs. For negative detunings $\Delta\omega < -25$ rad/ns, complex wave-mixing dynamics are observed in the two LP modes before the polarization switching, as shown in Figs. 13(b) and 13(c). Time-periodic oscillations in the LP mode intensities may bifurcate to period-doubling or even chaotic regimes in the route to the injection locking of the y-LP mode. In Fig. 13(d) is shown a small region of injection-locked steady state in the two LP modes, which corresponds to the EPIL steady state. This case of injection locking is found in a small range of negative detunings and destabilizes through a Hopf bifurcation. The Hopf bifurcation leads to a time-periodic modulation of the two LP modes, which may bifurcate to period-doubling or even chaotic regimes. For more negative detunings Figs. 13(e) and 13(f), the route to switching occurs through a complex cascade of time-periodic, period-doubling, and chaotic or quasiperiodic regimes, but the branch of the EPIL steady state does not appear anymore.

V. STABILITY ANALYSIS OF THE STEADY STATES

As shown in previous sections, our laser problem admits two different steady-state injection-locked solutions. One corresponds to injection locking of the y-LP mode, the x-LP mode being depressed, while the second steady state is a two-mode injection-locking solution with the two LP modes being locked to the master laser (EPIL steady state).

A mathematical expression for the y-LP injection-locked solution can be obtained directly from the rate equations (1)–(4). Introducing $F_{x,y}=R_{x,y}\exp(i\phi_{x,y})$ in Eqs. (1)–(4), the conditions for a steady-state injection-locked solution are given by

$$0=\kappa(1+i\alpha)[(D-1)R_x+idR_y\exp(i\Phi)]-i(\gamma_p+\Delta\omega)R_x-\gamma_aR_x, \tag{5}$$

$$0=\kappa(1+i\alpha)[(D-1)R_y-idR_x\exp(-i\Phi)]+i(\gamma_p-\Delta\omega)R_y+\gamma_aR_y+\kappa_{inj}E_{inj}^0\exp(-i\phi_y), \tag{6}$$

$$0=D(1+R_x^2+R_y^2)-\mu-2dR_xR_y\sin(\Phi), \tag{7}$$

$$0=-\gamma_sd-\gamma_e[d(R_x^2+R_y^2)-\mu]+2\gamma_eDR_xR_y\sin(\Phi), \tag{8}$$

where

$$\Phi=\phi_y-\phi_x. \tag{9}$$

The y-LP injection-locked solution corresponds to a case when $R_x=0$. From Eq. (5) this condition also implies $d=0$ if $R_y\neq 0$. We also obtain from Eqs. (6) and (7)

$$0=\kappa(1+i\alpha)(D-1)R_y+i(\gamma_p-\Delta\omega)R_y+\gamma_aR_y+\kappa_{inj}E_{inj}^0\times\exp(-i\phi_y), \tag{10}$$

$$0=D(1+R_y^2)-\mu. \tag{11}$$

Equation (11) then implies

$$D=\frac{\mu}{1+R_y^2}. \tag{12}$$

Introducing Eq. (12) into Eq. (10) leads to the new condition

$$0=\kappa(1+i\alpha)(\mu-1-R_y^2)\frac{R_y}{1+R_y^2}+i(\gamma_p-\Delta\omega)R_y+\gamma_aR_y+\kappa_{inj}E_{inj}^0\exp(-i\phi_y), \tag{13}$$

which is equivalent to

$$0=(\mu-1-R_y^2)\frac{R_y}{1+R_y^2}+\gamma_a\kappa^{-1}R_y+E_{inj}^0\cos(\phi_y), \tag{14}$$

$$0=\alpha(\mu-1-R_y^2)\frac{R_y}{1+R_y^2}+(\gamma_p-\Delta\omega)\kappa^{-1}R_y-E_{inj}^0\sin(\phi_y), \tag{15}$$

where we have considered as before $\kappa_{inj}=\kappa$.

Eliminating the trigonometric functions, we have

$$E_{inj}^{0^2}=R_y^2\left(\frac{\mu-1-R_y^2}{1+R_y^2}+\gamma_a\kappa^{-1}\right)^2+R_y^2\left(\alpha\frac{\mu-1-R_y^2}{1+R_y^2}+(\gamma_p-\Delta\omega)\kappa^{-1}\right)^2, \tag{16}$$

which gives the intensity solution R_y^2 as a function of the injection parameters P_{inj} and $\Delta\omega$ and of the laser parameters α, μ, κ, γ_a, and γ_p.

By contrast, the EPIL steady state is much more difficult to express mathematically, except for the particular case of a perfect resonance condition between the master frequency and the free-running x-LP mode frequency, i.e., for $\Delta\omega=-\gamma_p+\alpha\gamma_a$ [56]. As will be shown in the next figures, the EPIL steady-state branch is quite smooth for this resonant case but soon unfolds into more complicated shapes as we vary the detuning. On the other hand, numerical simulations only provide the stable part of the EPIL steady-state branch, and hence cannot provide the full branch of the steady-state solution. An alternative possibility to compute the complete branch of EPIL steady-state solutions is to use mathematical continuation methods, i.e., techniques to follow branches of solutions irrespective of their stability and starting from two initial branch points. We have therefore complemented our direct numerical simulations, which are based on numerical integration of the rate equations, with the use of continuation techniques available in the MATLAB package DDE-BIFTOOL [57]. DDE-BIFTOOL allows the continuation and stability analysis of steady states and time-periodic solutions for systems of ordinary or even delayed differential equations. We have used the continuation techniques not only to compute the complete branches of injection-locked steady states but also to compute their stability as a function of the laser and injection parameters. Bifurcation points on the steady-states are identified whenever an eigenvalue of the linearized, perturbed steady-state problem gets a positive real part. We can distinguish several kinds of bifurcations: a single real zero eigenvalue is an indication of either a saddle-node, pitchfork, or transcritical bifurcation while a pair of pure imaginary conjugated eigenvalues are associated with a Hopf bifurcation. The bifurcation points may be continued in the two-dimensional plane given by the injection strength and detuning parameters, and hence may lead to bifurcation lines or boundaries indicating in the map the regions of stable injection-locked solutions. The bifurcation lines may cross and lead to the so-called codimensional-2 bifurcation points, among which we find the Takens-Bogdanov bifurcation (a double-zero eigenvalue), the Gavrilov-Guckenheimer bifurcation (a single-zero eigenvalue in addition to a purely imaginary eigenvalue pair), and the double Hopf bifurcation (two purely imaginary eigenvalue pairs) [58].

Figure 14 shows the y-LP injection-locked solution and the EPIL solution as a function of the normalized injected power P_{inj}/I_0 together with information regarding their stability. Cases (a)–(f) correspond to different values of the detuning $\Delta\omega$. Stable (unstable) parts of the branches of steady states are indicated by thick (dotted) lines. For each steady-state solution, the x-LP (y-LP) mode intensity is plotted in black (gray). We also plot the bifurcation points on the steady-state branches: squares (□) are used for saddle-node bifurcations, stars (∗) indicate transcritical bifurcations, and diamonds (◇) indicate Hopf bifurcations. Bold diamonds emphasize the supercritical Hopf bifurcations, i.e., those Hopf points that modify the stability of the steady state branches. The other bifurcations located on unstable branches of steady states are called subcritical.

A particular case is Fig. 14(d) for which $\Delta\omega=\omega_x=-\gamma_p+\alpha\gamma_a$. As we increase the injected power above zero, a

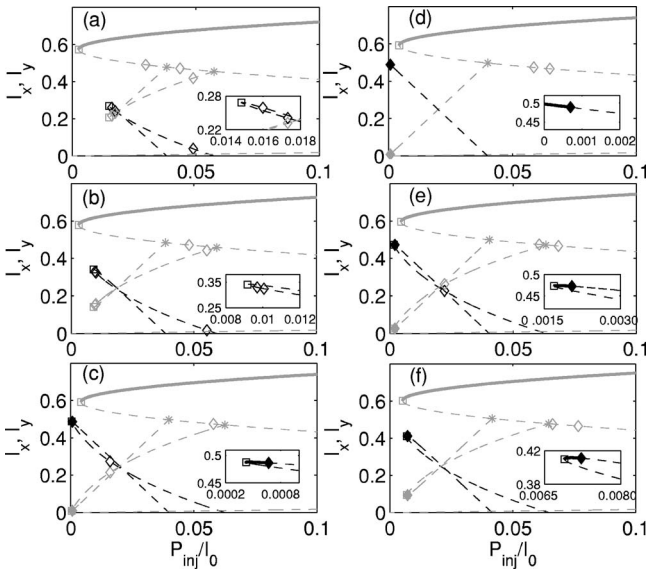

FIG. 14. Steady states of the laser system and their stability analysis for different values of the detuning $\Delta\omega$: $\Delta\omega$= (a) −16, (b) −20, (c) −28, (d) −28.5, (e) −30, and (f) −34 rad/ns. I_x (I_y) are plotted in black (gray) as a function of P_{inj}/I_0. Bifurcation points are plotted with symbols: squares (□) are used for saddle-node, stars (∗) for transcritical, and diamonds (◇) for Hopf bifurcations. Bold diamonds emphasize the supercritical Hopf bifurcations.

branch of EPIL steady states appears with I_x being larger than I_y. For a further increase of P_{inj}/P_0, this EPIL steady state destabilizes with a Hopf bifurcation leading to a stable time-periodic solution with the two LP modes lasing. As we have shown in previous sections, this time-periodic solution appearing from the EPIL steady state may further evolve to a period-doubling cascade, possibly leading to chaotic regimes. For a larger value of injected power, the only stable steady state is the y-LP injection-locked solution which appears from a saddle-node bifurcation. The node corresponds to the branch with the largest y-LP mode intensity, the x-LP mode being depressed. The smaller intensity branch corresponds to the saddle. The EPIL and y-LP solutions cross at a transcritical bifurcation. It is worth mentioning that two other Hopf bifurcations are found on the saddle branch of the y-LP injection-locked solution, as well as one Hopf bifurcation on the unstable EPIL branch.

When going to more negative detuning values than in Fig. 14(d) the EPIL solution suddenly unfolds and a saddle-node bifurcation now leads to two branches of solutions for each of the LP modes [Fig. 14(e)]. The stable solution corresponds to the node, which is the solution with the largest I_x and the smallest I_y values. The second solution corresponds to the saddle branch. The node destabilizes with a supercritical Hopf bifurcation leading to stable time-periodic solution with the two LP modes lasing. The case Fig. 14(e) is in fact the same as the bifurcation diagram of Fig. 2 but showing both stable and unstable branches of steady states. Very interestingly, the saddle-node bifurcation on the EPIL steady state might be located at a larger value than the saddle node on the y-LP injection-locked solution, as shown in Fig. 14(f). In that case, there is a range of injected powers for which a bistability exists between a stable EPIL solution and a stable y-LP injection-locked solution. As will be shown in the next figures, the range of $\Delta\omega$ in which this bistability exists is limited by a codimension-2 Gavrilov-Guckenheimer bifurcation. We can already see in Fig. 14(e) that the Hopf bifurcation on EPIL solution moves towards the saddle-node bifurcation as $\Delta\omega$ goes to more negative values. This bistability case between two injection-locked solutions therefore complements the bistability between the y-LP injection-locked solution and complex dynamics emerging from the EPIL Hopf bifurcation, as shown in Fig. 2 [or equivalently Fig. 14(e)].

When going to more positive detuning values than in Fig. Fig. 14(d), a similar unfolding mechanism occurs with a saddle-node bifurcation appearing on the EPIL solution. In Fig. 14(c), a stable branch of EPIL solution is still found and corresponds to the node branch. It again destabilizes with a supercritical Hopf bifurcation to a stable time-periodic dynamics. As we still increase the detuning, the stability of the EPIL solution is lost as soon as the Hopf bifurcation coalesces with the saddle-node bifurcation. For detuning values beyond this codimension-2 bifurcation, the Hopf bifurcation determining the stability of the EPIL steady state is now on the saddle branch and the EPIL solution is then completely unstable [Figs. 14(a) and 14(b)].

We have also followed the saddle-node, transcritical, and Hopf bifurcation points in the two-dimensional plane given by the injection parameters P_{inj}/I_0 and $\Delta\omega$; see Fig. 15. Bifurcations on the y-LP injection-locked solution are plotted in blue and are labeled as H_y^1, H_y^2, and H_y^3 for the Hopf bifurcations and F_y^1 for the fold bifurcation. Bifurcations on the EPIL solution are plotted in red, and are labeled H_{xy}^1, H_{xy}^2 for the Hopf bifurcations and F_{xy}^1, F_{xy}^2 for the fold bifurcations. Supercritical (subcritical) bifurcations are indicated by solid (dashed) lines. T is a transcritical bifurcation. Codimension-2 bifurcations are shown with circles (●) for a Gavrilov-Guckenheimer bifurcation, triangles (▲) for a double Hopf point, and stars for a Takens-Bogdanov bifurcation. The empty circles (○) indicate codimension-3 bifurcations.

This figure allows us to get insight into the stability conditions on the injection-locked steady states. The y-LP injection-locked solution appears from the saddle-node bifurcation F_y^1 and destabilizes with the supercritical Hopf bifurcation H_y^1, which then leads to a stable time-periodic dynamics with only the y-LP mode lasing. A codimension-2 Gavrilov-Guckenheimer bifurcation is located at G_3 where the Hopf and saddle-node bifurcations merge. Point G_3 is located very close to $\Delta\omega \sim \gamma_p - \alpha\gamma_a$, i.e., for $\omega_{inj} \sim \omega_y$. This detuning value is also the one for which the polarization switching requires the minimum injected power, as shown in Fig. 11. For detunings larger than G_3, the injection-locked solution is found for much larger values of the injection strength, once the laser system crosses the bifurcation line H_y^1 which then corresponds to an inverse Hopf bifurcation. The EPIL solution on the other hand only exists in a quite small range of detuning values centered around $\Delta\omega = \gamma_p + \alpha\gamma_a$. Except for that particular detuning value, the EPIL solution appears from a saddle-node bifurcation F_{xy}^1 or F_{xy}^2. As we increase the injected power, it destabilizes with the Hopf bifurcation H_{xy}^1. The range of detunings in which one can

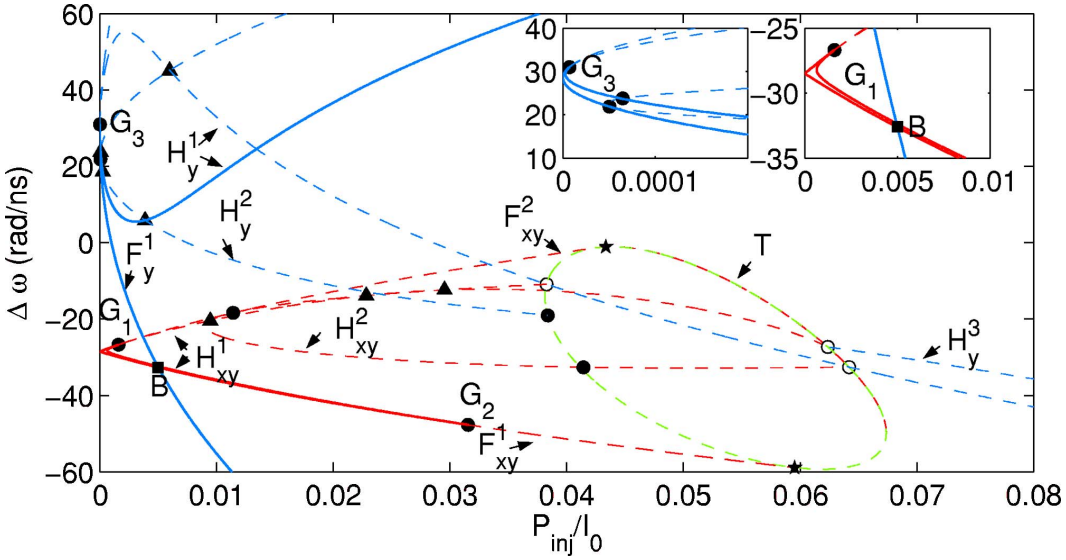

FIG. 15. (Color online) Mapping of the steady-state stability boundaries in the plane of the injection parameters $(P_{inj}/I_0, \Delta\omega)$. Bifurcations on the y-LP injection-locked solution are plotted in blue and are labeled as H^1_y, H^2_y, and H^3_y for the Hopf bifurcations and F^1_y for the fold bifurcation. Bifurcations on the EPIL solution are plotted in red, and are labeled H^1_{xy}, H^2_{xy} for the Hopf bifurcations and F^1_{xy}, F^2_{xy} for the fold bifurcations. Supercritical (subcritical) bifurcations are indicated by solid (dashed) lines. T is a transcritical bifurcation. Codimension-2 bifurcations are shown with circles (●) for a Gavrilov-Guckenheimer bifurcation, triangles (▲) for a double Hopf point, and stars for a Takens-Bogdanov bifurcation. The empty circles (○) indicate co-dimension three bifurcations. Points B, G_1, G_2, and G_3 are particular points discussed in the text. (b) and (c) are enlargements of parts of the map shown in (a).

find a stable EPIL solution is delimited by two codimension-2 Gavrilov-Guckenheimer points G_1 and G_2 at which the saddle-node and the Hopf bifurcation lines become tangent. This detailed stability map also sheds light into a possible bistability between the EPIL solution and the y-LP injection-locked solution, as shown in Fig. 14(f). The saddle-node bifurcation on EPIL solution F^1_{xy} and the saddle-node bifurcation on the y-LP mode solution F^1_y intersect at the point B. For detuning values between B and G_2 a stable EPIL solution coexists in a small range of injection strength with the y-LP injection-locked steady state. Bistability between two injection-locked solutions has also been reported in a single-mode edge-emitting laser with optical injection, for a low pump and/or small value of α and for a rather large value of the injection strength [59,60]. However, that bistability case is of different dynamical origin from the one we report in this paper. Moreover, in our case the two injection-locked solutions are associated with different polarization properties. Other bifurcation lines are shown in Fig. 15 and correspond to subcritical bifurcations, i.e., which appear on unstable branches of steady states. These subcritical bifurcations are connected to the supercritical bifurcations and to other subcritical bifurcations through codimension-2 or even codimension-3 bifurcations. The transcritical bifurcation line plays a central role in organizing the bifurcations for negative detunings.

As mentioned before, the EPIL solution is centered around what seems to be a particular resonance condition for which $\Delta\omega = -\gamma_p + \alpha\gamma_a$, i.e. for which the master laser frequency is close to the free-running x-LP mode frequency. The existence of such a resonance condition is further confirmed in Fig. 16 for which the saddle-node and Hopf bifurcation boundaries of the EPIL solution are shown for two different values of the linear birefringence parameter γ_p. As γ_p increases and the two LP mode frequency splitting therefore increases, the region of stable EPIL solutions moves toward more negative detuning values and the saddle-node bifurcation lines again intersect at the perfect resonance condition $\Delta\omega = -\gamma_p + \alpha\gamma_a$. We have also tested modifications of α and γ_a and in all cases this EPIL solution is indeed related to the existence of a resonance between the master laser frequency and the free-running frequency of the normally depressed mode.

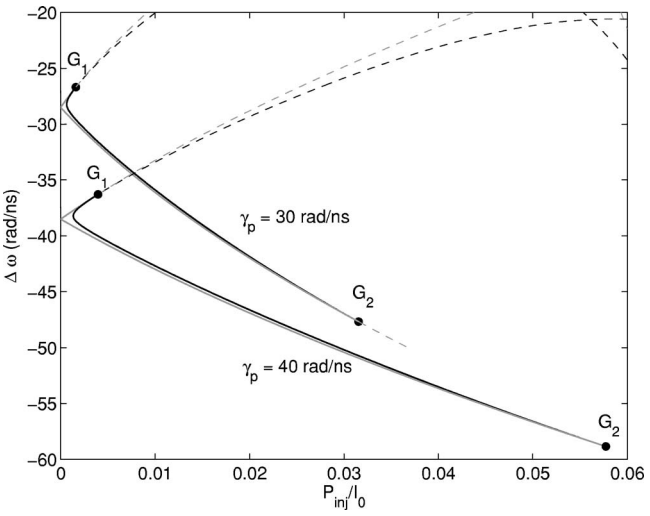

FIG. 16. Mapping of the stability boundaries of the EPIL solution in the plane of the injection parameters $(P_{inj}/I_0, \Delta\omega)$ and for two different values of γ_p. Saddle-node (Hopf) bifurcations are plotted in gray (black). Solid (dashed) lines indicate supercritical (subcritical) bifurcations.

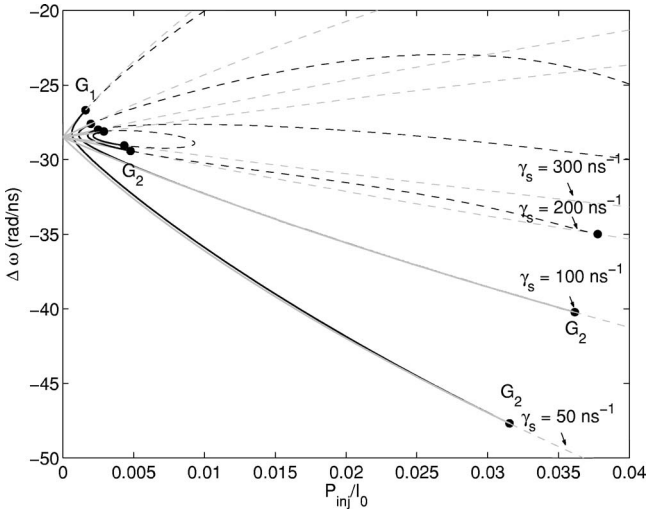

FIG. 17. Mapping of the stability boundaries of the EPIL solution in the plane of the injection parameters $(P_{inj}/I_0, \Delta\omega)$ for increasing values of γ_s. Saddle-node (Hopf) bifurcations are plotted in gray (black). Solid (dashed) lines indicate supercritical (subcritical) bifurcations.

Equation (16) shows that the y-LP injection-locked solution depends of course on the injection parameters and some of the laser parameters (α, μ, κ, γ_a, and γ_p) but not on the spin-flip relaxation rate γ_s. The EPIL solution and its stability boundaries are on the other hand strongly dependent on γ_s, as shown in Fig. 17. As γ_s increases, the range of detuning values in which one can find a stable EPIL (between points G_1 and G_2) progressively decreases. Moreover, interestingly the increase of γ_s first pushes the codimension-2 point G_2 to larger values of injection strength (for $\gamma_s = 100\ \mathrm{ns}^{-1}$) but then, for larger γ_s, two Gavrilov-Guckenheimer points appear on the saddle-node branch and the point G_2 that shows the end of the stable EPIL region is strongly shifted to smaller values of injected power. The range of parameters in which one can find a two-mode injection-locked solution then quickly shrinks as γ_s increases but is not null. The spin-flip relaxation rate γ_s is an important ingredient in the framework of the SFM model. It aims at modeling several microscopic mechanisms that are responsible for the relaxation of the electron spin in quantum well semiconductor materials. In comparisons between experiments and theory based on SFM model, the γ_s parameter is usually considered as a fitting parameter since its direct measurement is very difficult at room temperature and for the high levels of carrier density encountered in lasing operation. Reported values of γ_s from experimental fittings of different VCSEL devices range from $\gamma_s \simeq 20\ \mathrm{ns}^{-1}$ [61], $\gamma_s \simeq 100\ \mathrm{ns}^{-1}$ [62], $\gamma_s > 300\ \mathrm{ns}^{-1}$ [63], or even $\gamma_s \simeq \infty$ [64]. Our results suggest that an indirect measurement of γ_s might be possible by detecting experimentally the boundaries of the two-mode injection-locking steady states in optically injected VCSELs and by fitting the stability analysis as a function of γ_s. The dynamics of optically injected VCSELs might therefore give hints to the importance of spin-flip relaxation mechanisms in the VCSEL devices under study and might also provide alternative ways to determine a value of the related γ_s parameter.

VI. CONCLUSIONS

In summary, we have reported the polarization dynamics accompanying the route to polarization switching in optically injected VCSELs. The polarization switching typically consists of a cascade of bifurcations with cascaded wave mixing for smaller values of the injection strength, then time-periodic, period-doubling, and even chaotic regimes in the two LP modes before the laser switches to the injection-locked steady state with the master polarization. For some detuning values (such that the master laser frequency is close to the free-running frequency of the depressed LP mode), the slave VCSEL may exhibit a stationary regime for which the two LP modes both lock to the master laser and hence the VCSEL emits an elliptically polarized injection-locked steady state. This two-mode injection-locked solution is unusual in this optical injection problem and its bifurcation boundaries have been determined thanks to numerical continuation methods. Codimension-2 Gavrilov-Guckenheimer bifurcation points organize the stability of the EPIL solution and are robust against large variations of the laser parameters. They result from the interaction between the unfolding of the EPIL solution as the detuning varies, i.e., the existence of saddle-node bifurcations, and the existence of a Hopf bifurcation at larger values of the injection strength. Moreover, there is a detuning range for which an additional bistability may occur between the EPIL steady state and the solution that is injection locked with the master polarization. Our detailed mapping and steady-state bifurcation analysis provide further light on a two-mode injection-locking problem and motivate further experiments. The search for an EPIL solution might give indications of the value of the spin-flip relaxation rate of the VCSEL device under study, i.e., it might confirm the importance or not of spin relaxation mechanisms in the rate equation modeling. Finally, analytical studies of the EPIL solution and its stability conditions can be performed in the light of our results and might shed light on the two-mode optical injection dynamics.

ACKNOWLEDGMENTS

The authors would like to thank Thomas Erneux for many fruitful and stimulating discussions on injection-locked solutions. The authors acknowledge the support of the IAP "Photon" program of the Belgian government, as well as FWO-Flanders, GOA and OZR of the VUB, the Région Lorraine (France), the EU-IST SLAM project, and the COST 288 European Action.

[1] J. Sacher, W. Elsäßer, and E. Gobel, Phys. Rev. Lett. **63**, 2224 (1989).
[2] Y. C. Chen, H. G. Winful, and J. M. Liu, Appl. Phys. Lett. **47**, 208 (1985).
[3] R. Lang and K. Kobayashi, IEEE J. Quantum Electron. **QE-16**, 347 (1980).
[4] V. Kovanis, A. Gavrielides, T. B. Simpson, and J. M. Liu, Appl. Phys. Lett. **67**, 2780 (1995).
[5] S. Strogatz, *Nonlinear Dynamics and Chaos* (Addison-Wesley, Reading, MA, 1994).
[6] C. R. Mirasso, P. Colet, and P. Garcia-Fernandez, IEEE Photonics Technol. Lett. **8**, 299 (1996).
[7] S. Sivaprakasam and K. A. Shore, Opt. Lett. **24**, 466 (1999).
[8] I. Fischer, Y. Liu, and P. Davis, Phys. Rev. A **62**, 011801(R) (2000).
[9] S. Jiang, Z. Pan, M. Dagenais, R. A. Morgan, and K. Kojima, Appl. Phys. Lett. **63**, 3545 (1993).
[10] A. Tager and K. Petermann, IEEE J. Quantum Electron. **QE-30**, 1553 (1994).
[11] F. Robert, P. Besnard, M. L. Charès, and G. Stéphan, IEEE J. Quantum Electron. **QE-33**, 2231 (1997).
[12] H. Li, A. Hohl, A. Gavrielides, H. Hou, and K. D. Choquette, Appl. Phys. Lett. **72**, 2355 (1998).
[13] M. Sciamanna, T. Erneux, F. Rogister, O. Deparis, P. Mégret, and M. Blondel, Phys. Rev. A **65**, 041801(R) (2002).
[14] M. Sciamanna, F. Rogister, O. Deparis, P. Mégret, M. Blondel, and T. Erneux, Opt. Lett. **27**, 261 (2002).
[15] T. Erneux, A. Gavrielides, and M. Sciamanna, Phys. Rev. A **66**, 033809 (2002).
[16] M. Sciamanna, Ph.D. thesis, Faculté Polytechnique de Mons, Belgium, 2004 (unpublished).
[17] O. Ushakov, S. Bauer, O. Brox, H.-J. Wünsche, and F. Henneberger, Phys. Rev. Lett. **92**, 043902 (2004).
[18] S. Piazzolla, P. Spano, and M. Tamburrini, IEEE J. Quantum Electron. **22**, 2219 (1986).
[19] T. B. Simpson, J. M. Liu, and A. Gavrielides, IEEE Photonics Technol. Lett. **7**, 709 (1995).
[20] J. M. Liu, H. F. Chen, X. J. Meng, and T. B. Simpson, IEEE Photonics Technol. Lett. **9**, 1325 (1997).
[21] K. Iga, IEEE J. Sel. Top. Quantum Electron. **6**, 1201 (2000).
[22] C. J. Chang-Hasnain, J. P. Harbison, G. Hasnain, A. C. Von Lehmen, L. T. Florez, and N. G. Stoffel, IEEE J. Quantum Electron. **27**, 1402 (1991).
[23] C. Masoller and N. B. Abraham, Phys. Rev. A **59**, 3021 (1999).
[24] M. Giudici, S. Balle, T. Ackemann, S. Barland, and J. R. Tredicce, J. Opt. Soc. Am. B **16**, 2114 (1999).
[25] M. Sciamanna, C. Masoller, N. B. Abraham, F. Rogister, P. Mégret, and M. Blondel, J. Opt. Soc. Am. B **20**, 37 (2003).
[26] M. Sciamanna, C. Masoller, F. Rogister, P. Mégret, N. B. Abraham, and M. Blondel, Phys. Rev. A **68**, 015805 (2003).
[27] M. Sondermann, H. Bohnet, and T. Ackemann, Phys. Rev. A **67**, 021802(R) (2003).
[28] C. Masoller, Phys. Rev. Lett. **90**, 020601 (2003).
[29] M. Sciamanna, K. Panajotov, H. Thienpont, I. Veretennicoff, P. Mégret, and M. Blondel, Opt. Lett. **28**, 1543 (2003).
[30] K. Panajotov, M. Sciamanna, A. Tabaka, P. Mégret, M. Blondel, G. Giacomelli, F. Marin, H. Thienpont, and I. Veretennicoff, Phys. Rev. A **69**, 011801(R) (2004).
[31] J. Houlihan, D. Goulding, Th. Busch, C. Masoller, and G. Huyet, Phys. Rev. Lett. **92**, 050601 (2004).
[32] A. Valle, L. Pesquera, S. I. Turovets, and J. M. Lopez, Opt. Commun. **208**, 173 (2002).
[33] M. Sciamanna, A. Valle, P. Megret, M. Blondel, and K. Panajotov, Phys. Rev. E **68**, 016207 (2003).
[34] Z. G. Pan, S. Jiang, M. Dagenais, R. A. Morgan, K. Kojima, M. T. Asom, R. E. Leibenguth, G. D. Guth, and M. W. Focht, Appl. Phys. Lett. **63**, 2999 (1993).
[35] K. Panajotov, F. Berghmans, M. Peeters, G. Verschaffelt, J. Danckaert, I. Veretennicoff, and H. Thienpont, IEEE Photonics Technol. Lett. **11**, 985 (1999).
[36] D. L. Boiko, G. M. Stéphan, and P. Besnard, J. Appl. Phys. **86**, 4096 (1999).
[37] H. Li, T. L. Lucas, J. G. McInerney, M. W. Wright, and R. A. Morgan, IEEE J. Quantum Electron. **32**, 227 (1996).
[38] S. Jiang, M. Dagenais, and R. A. Morgan, Appl. Phys. Lett. **65**, 1334 (1994).
[39] T. B. Simpson, J. M. Liu, K. F. Huang, and K. Tai, Quantum Semiclassic. Opt. **9**, 765 (1997).
[40] Y. Hong, P. S. Spencer, S. Bandyopadhyay, P. Rees, and K. A. Shore, Opt. Commun. **216**, 185 (2003).
[41] J. Y. Law, G. H. M. van Tartwijk, and G. P. Agrawall, Opt. Commun. **9**, 737 (1997).
[42] Y. Hong, P. S. Spencer, P. Rees, and K. A. Shore, IEEE J. Quantum Electron. **38**, 274 (2002).
[43] M. S. Torre, C. Masoller, and K. A. Shore, IEEE J. Quantum Electron. **40**, 25 (2004).
[44] B. Lücke, G. Hergenhan, U. Brauch, and A. Giesen, IEEE Photonics Technol. Lett. **13**, 100 (2001).
[45] Y. Onishi, N. Nishiyama, C. Caneau, F. Koyama, and C. Zah, IEEE Photonics Technol. Lett. **16**, 1236 (2004).
[46] C.-H. Chang, L. Chrostowski, and C. J. Chang-Hasnain, IEEE Photonics Technol. Lett. **14**, 1635 (2002).
[47] L. Chrostowski, C.-H. Chang, and C. J. Chang-Hasnain, IEEE Photonics Technol. Lett. **15**, 498 (2003).
[48] C.-H. Chang, L. Chrostowski, and C. J. Chang-Hasnain, IEEE J. Sel. Top. Quantum Electron. **9**, 1386 (2003).
[49] L. Chrostowski, C.-H. Chang, and C. J. Chang-Hasnain, IEEE Photonics Technol. Lett. **15**, 498 (2004).
[50] J. Martin-Regalado, F. Prati, M. San Miguel, and N. B. Abraham, IEEE J. Quantum Electron. **33**, 765 (1997).
[51] M. San Miguel, Q. Feng, and J. V. Moloney, Phys. Rev. A **52**, 1728 (1995).
[52] B. S. Ryvkin, K. Panajotov, E. A. Avrutin, I. Veretennicoff, and H. Thienpont, J. Appl. Phys. **96**, 6002 (2004).
[53] G. H. M. Van Tartwijk, G. Mujires, D. Lenstra, M. P. Van Exter, and J. P. Woerdman, Electron. Lett. **29**, 137 (1993).
[54] T. B. Simpson, J. M. Liu, K. F. Huang, and K. Tai, Quantum Semiclassic. Opt. **9**, 765 (1997).
[55] S. Wieczorek, B. Krauskopf, and D. Lenstra, Opt. Commun. **172**, 279 (1999).
[56] T. Erneux (private communication).
[57] K. Engelborghs, T. Luzyanina, and G. Samaey, computer code DDE-BIFTOOL version 2.00, http://www.cs.kuleuven.ac.be/cwis/research/twr/research/software/delay/ddebiftool.shtml
[58] J. Guckenheimer, P. Holmes, and F. John, *Nonlinear Oscillations, Dynamical Systems, and Bifurcations of Vector Fields* (Springer-Verlag, Berlin, 1997).

[59] T. Erneux, A. Gavrielides, and V. Kovanis, Quantum Semiclassic. Opt. **9**, 811 (1997).
[60] S. Wieczorek, Ph.D. thesis, Vrije Universiteit, Amsterdam, The Netherlands, 2002 (unpublished).
[61] M. Sondermann, M. Weinkath, T. Ackemann, J. Mulet, and S. Balle, Phys. Rev. A **68**, 033822 (2003).
[62] M. P. Van Exter, M. B. Willemsen, and J. P. Woerdman, Phys. Rev. A **58**, 4191 (1998).
[63] R. F. M. Hendriks, M. P. Van Exter, J. P. Woerdman, K. H. Gulden, and M. Moser, IEEE J. Quantum Electron. **34**, 1455 (1998).
[64] P. Besnard, M.-L. Charés, G. Stéphan, and F. Robert, J. Opt. Soc. Am. B **16**, 1059 (1999).